Semiconductor Electrodes

LVII. Differential Photocurrent and Second Harmonic Techniques for *in situ* Monitoring of Surface States on n-$MoSe_2$ in Aqueous Solutions

Bob L. Wheeler, G. Nagasubramanian, and Allen J. Bard*

Department of Chemistry, The University of Texas at Austin, Austin, Texas 78712

ABSTRACT

Second harmonic ac impedance and differential photocurrent techniques are employed to monitor, *in situ*, the surface states on n-$MoSe_2$ electrodes in aqueous solutions containing the $Fe(CN)_6^{3-/4-}$ couple. These two techniques are qualitatively more sensitive to the presence of surface states on single-crystal n-$MoSe_2$ than first harmonic ac techniques. Surface states on this semiconductor electrode were passivated by a thin layer of RuO_x. This film also increased the PEC efficiency of both single-crystal and polycrystalline n-$MoSe_2$.

Surface states, either intrinsic or extrinsic, are known to affect the performance of photoelectrochemical (PEC) cells and behavior of semiconductor electrodes by promoting Fermi level pinning, acting as recombination centers, and abetting dark current flow (1-3). Several techniques for the study of surface states at electrode surfaces contacting electrolyte solutions are available; these include (*i*) current-potential methods (3), (*ii*) photocapacitance spectroscopy (4), (*iii*) electroluminescence spectroscopy (5-7), (*iv*) photoluminescence spectroscopy (7), (*v*) measurements of the subbandgap photoresponse (8-10), (*vi*) interfacial capacitance (11), and (*vii*) surface photovoltage (12). Recently, we reported that the ac impedance technique can provide information about both the energy distribution and density of surface states (13, 14). This method could detect the presence of surface states even when their density was too small to cause Fermi level pinning on n-$MoTe_2$. We report here ac impedance studies of n-$MoSe_2$ and demonstrate the use of this method as a means of *in situ* monitoring of the semiconductor surface and the effects of surface treatments. In addition, two techniques are described which are qualitatively even more sensitive to the presence of surface states: the second harmonic ac impedance and the differential photocurrent techniques. Deposition of a thin layer of RuO_x on the surface of n-$MoSe_2$ was shown by all three techniques to passivate the surface states present. Concurrently, the photocurrent-voltage behavior showed a dramatic improvement. This provides strong evidence that all three techniques monitor the semiconductor surface, *in situ*, and that the surface states were responsible for the poor photocurrent-voltage behavior with the untreated surface. The improvement of the single-crystal behavior encouraged us to attempt to improve polycrystalline $MoSe_2$ films by the same method.

Experimental

Electrodes.—Single crystals of n-$MoSe_2$[1] were used. The van der Waals surface ($\perp$ C axis) was the face exposed to the solution. Ohmic contacts were made to the back surfaces with Ga/In eutectic. A copper wire lead for electrical contact was attached to the ohmic contacts with silver conductive paint (Allied Product Corporation, New Haven, Connecticut) and then covered with 5 min epoxy cement (Devcon Corporation, Danvers, Massachusetts). A fresh surface was exposed by peeling off the top van der Waals layers with adhesive tape until the surface appeared free of edges or steps upon examination with a microscope. Assemblies were then mounted in 6 mm diam glass tubing and held in place by covering all except the front surface with silicone rubber sealant (Dow Corning Corporation, Midland, Michigan), which also served as a seal against the seepage of the electrolyte to the back contact. The exposed area was ~0.06 cm^2 for all electrodes used. The surfaces of the electrodes were treated with 6*M* HCl for 1 min and rinsed with distilled water prior to use. The electrolyte consisted of an aqueous solution of 0.2*M* $K_2Fe(CN)_6$, adjusted to *p*H 8 with KOH, and deaerated with prepurified N_2 prior to the experiment. A positive pressure of this N_2 was kept in the cell during the experiments.

Polycrystalline films of $MoSe_2$ were made from $MoSe_2$ powder, 99+% (Alfa, Danvers, Massachusetts) using I_2 vapor transport. A quartz tube, 1.5 cm diam + 15 cm length, was rinsed successively with 48% HF, distilled water, aqua regia, distilled water, 48% HF, and distilled water, then dried under vacuum at 150°C. Approximately 3g of the $MoSe_2$ powder was placed in the tube, and the tube was evacuated ($< 10^{-5}$ torr) for 1h. The tube was filled with He and I_2 was quickly added (~20 mg/g $MoSe_2$). Most of the He was removed and the tube was cooled in liquid N_2 and evacuated and sealed. The $MoSe_2$ and I_2 were distributed along the tube, which was placed in a split tube furnace (Hevi-duty Electric Company, Watertown, Wisconsin, length 18 in., diam 1.25 in.) and kept at 900°C. The ends of the furnace were plugged with spun alumina to minimize any temperature gradient which could cause growth of single crystals. After three weeks, the tube was removed from the furnace, and a suitable section was cooled under running water to condense the I_2, and then the rest of the tube was cooled. A polycrystalline mass of $MoSe_2$ had grown above and beneath the original charge. The side of the polycrystalline mass which faced the center of the quartz tube was covered with crystalline platelets protruding perpendicularly to the quartz walls; this was designated as the rough side. The opposite side, which was against the quartz tube, was shiny and was designated as the smooth side. The polycrystalline films were quite sturdy and could be removed easily from the quartz after the tube was broken. Contact to these films was made with silver paint and copper wire. The contact and the rest of the film, except for the area to be exposed to the solution, was covered with 5 min epoxy cement. Since the films had pinholes, the contact had to be kept above the solution level. The electrolyte solution used was an aqueous solution of 1*M* KBr, deaerated with N_2.

A conventional three-electrode single-compartment cell with a flat Pyrex window for illumination of the semiconductor electrode was used. The cell, which had a volume of about 30 ml, also contained a Pt gauze electrode (area > 40 cm^2) which was used as the counterelectrode. The reference electrode was a saturated calomel electrode (SCE) separated from the cell by a KCl-saturated agar bridge. All potentials are reported *vs.* SCE.

Current-potential behavior was obtained with a PAR Model 173 potentiostat with Model 179 digital coulometer plug-in and Model 175 programmer (Princeton Applied Research, Princeton, New Jersey) and recorded with a Model 2000 X-Y recorder (Houston Instruments, Austin, Texas). Polychromatic illumination was obtained from a

*Electrochemical Society Active Member.

[1]The single crystals of n-$MoSe_2$ were obtained from Dr. Barry Miller and Dr. Frank DiSalvo of AT&T Bell Laboratories, Murray Hill, New Jersey.

450W Xe lamp (Oriel Corporation, Stamford, Connecticut) provided with a water filter. The intensity was 100 mW/cm^2.

Photodeposition of RuO_x ($x \leq 2$) on the $MoSe_2$ electrodes was accomplished by a modification of the procedure reported by Anderson and Warren (15). To a solution of 1.7g of $RuCl_3 \cdot 3H_2O$ in 100 ml of 98% aqueous EtOH, 6 ml of 1,3-cyclohexadiene was added (16). The solution was placed in a boiling flask fitted with a reflux condenser and heated to 45°C for 3h. The reflux condenser was then removed, and the solution volume was reduced to 30 ml. The red precipitate of $[Ru(\eta^6\text{-}C_6H_6)Cl_2]_2$ was collected by filtration, washed with EtOH, and allowed to dry in air. This species was dissolved in a minimum amount of water, and 4 mol $AgBF_4$ were added per mole of Ru dimer to obtain $Ru(\eta^6\text{-}C_6H_6)(OH_2)_3^{2+}$ and a precipitate of AgCl. The solution was filtered, and the filtrate was diluted to give 0.04*M* Ru. The *p*H was adjusted to 5 and $NaClO_4$ was used as supporting electrolyte at a concentration of 0.1*M*. The aquated species can be oxidized on Pt at +0.9V *vs.* SCE to give a film of RuO_x (15). On illuminated n-$MoSe_2$, photo-oxidation starts at +0.2V *vs.* SCE. The films were produced by illuminating the n-$MoSe_2$ with white light and biasing at +0.5V while monitoring the charge passed with a coulometer.

AC impedance.—The lock-in technique (13, 14) was used to measure the ac impedance behavior as a function of applied potential. In this technique, a small amplitude sine wave, 12 mV peak to peak, from a wide-range oscillator (Model 200 CD, Hewlett-Packard, Palo Alto, California) is superimposed on a slow (≤ 5 mV/s) dc ramp from the PAR universal programmer by the PAR potentiostat and applied to the cell. The output of the current follower of the potentiostat is input to a lock-in amplifier (PAR Model 5204 or 5206) which separates the signal into the components in and out of phase (90°) with the ac signal from the oscillator. These signals were calibrated by using an RC circuit composed of a resistance substitution box checked with a digital multimeter and a precision decade capacitor (Hewlett-Packard Model 4440 B). The in and out of phase signals as a function of dc potential were plotted on an X-Y-Y recorder (Soltec, Sun Valley, California, Model 6432).

The second harmonic measurements were made by applying the same ac signal at a fundamental frequency (*f*) and setting the lock-in on the external 2*f* mode. The HP200 CD oscillator was found to have negligible harmonic distortion detectable at the sensitivities used, and, therefore, this oscillator was used for all ac measurements. All other instrumentation was the same as that used in the measurements at the fundamental frequency.

Differential photocurrent.—In this technique, the photocurrent is electronically differentiated with respect to potential as a function of potential (17). The method used the intermodulation frequency of chopped light and ac modulation of the electrode. This method has been described in detail elsewhere (18) and the results are plots of the photocurrent *vs.* voltage, as well as the differential photocurrent *vs.* voltage. Instrumentation is identical to that described previously (18).

Results and Discussion

Capacitance-voltage behavior of single-crystal n-$MoSe_2$.—Mott-Schottky (M-S) plots over the frequency range (*f*) 0.5-5 kHz are given in Fig. 1 for n-$MoSe_2$ in aqueous solution containing $Fe(CN)_6^{4-/3-}$ as the redox couple. In this frequency regime, the capacitance values (*C*) were generally free from the deleterious effects of surface states and yielded values of *C* which were only slightly dependent on *f*. The value of flatband potential (V_{FB}) and the average value of the doping density (N_D) obtained from the M-S plots are around −0.1V *vs.* SCE and 2 × 10^{17}/cm^3. Taking the bandgap as 1.4 eV (19), we estimate that the valance band (VB) and conduction band (CB) edges are located, respectively, at +1.16 and −0.24V.

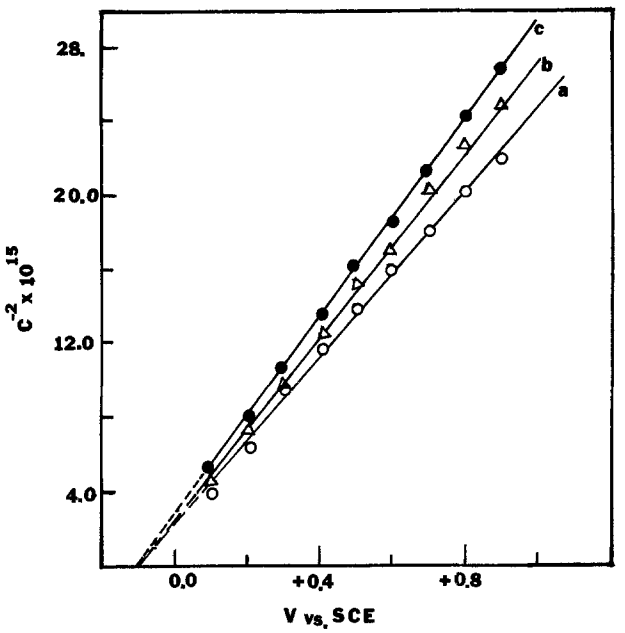

Fig. 1. Mott-Schottky plots for n-$MoSe_2$ in aqueous 0.2*M* $K_4Fe(CN)_6$. a: 500 Hz. b: 1 kHz. c: 5 kHz.

Inflections in the reverse bias region of capacitance (*C*) or conductance (*G*) *vs.* *V* plots are often associated with excess charge residing in surface states (20). Such inflections will be manifested as dips or humps in the C-V or G-V plots with frequency-dependent peak positions and heights. The shape and size of the humps are determined by the time constant (τ) associated with charge exchange and the density distribution as a function of potential energy (N_{ss}, cm^{-2}eV^{-1}). The integrated area under the hump can be used to obtain quantitative information about the total density of surface states. This approach was used previously (14) to obtain a surface-state density of 1.4 × 10^{10} cm^{-2} for n-$MoSe_2$. This density is too small for pinning the Fermi level (21, 22). In Fig. 2 are shown plots of the equivalent parallel conductance (G_p) and equivalent parallel capacitance (C_p) *vs.* *V* for two typical n-$MoSe_2$ electrodes in aqueous solution containing 0.2*M* $K_4Fe(CN)_6$ at two different frequencies, 100 and 500 Hz. While the C_p *vs.* *V* plots at 500 Hz show no hump in contrast to that at 100 Hz, the G_p *vs.* *V* plots exhibit humps with a frequency-dependent peak height. Different electrodes all gave similar results. This observation, that the in-phase component is more sensitive to the presence of surface states than the 90° component, is in accord with earlier observations (13, 23, 24). In Fig. 3 is shown the second harmonic of the ac impedance of n-$MoSe_2$ electrode of Fig. 2a in 0.2*M* $K_4Fe(CN)_6$ with ac modulation at 500 Hz. Note the absence of any dip or hump in the C_p *vs.* *V* at 500 Hz, while the second harmonic (which is related to dC/dV *vs.* *V*) exhibits a hump around +0.2V, roughly in the same potential region in which G_p *vs.* *V* exhibits a hump. In many devices, the capacitance changes much less rapidly than dC/dV (25, 26, 27) since, while $C_p \propto V^{1/2}$, $dC_p/dV \propto V^{-3/2}$. As with the dC_p/dV behavior, the small hump present in the G_p *vs.* *V* curve is greatly amplified in the second harmonic of the conductance (dG_p/dV) (Fig. 3).

Photocurrent and differential photocurrent behavior of n-$MoSe_2$.—In Fig. 4 are given the photocurrent (*j*) and the differential photocurrent (Δj) *vs.* *V* for two n-$MoSe_2$ electrodes with monochromatic illumination at 500 nm in aqueous solution containing $K_4Fe(CN)_6$ as redox couple. The plots in Fig. 4a are for the same electrode as Fig. 2a. Note that the current axis for Δj is given in a logarithmic scale. The log Δj *vs.* *V* plots exhibit a large hump in the potential regime in which *j* *vs.* *V* curves exhibit a dip. Similar results were obtained when the two modulating frequencies were varied by ± 20% while maintaining the intermodulation frequency constant at 400 Hz for ease of

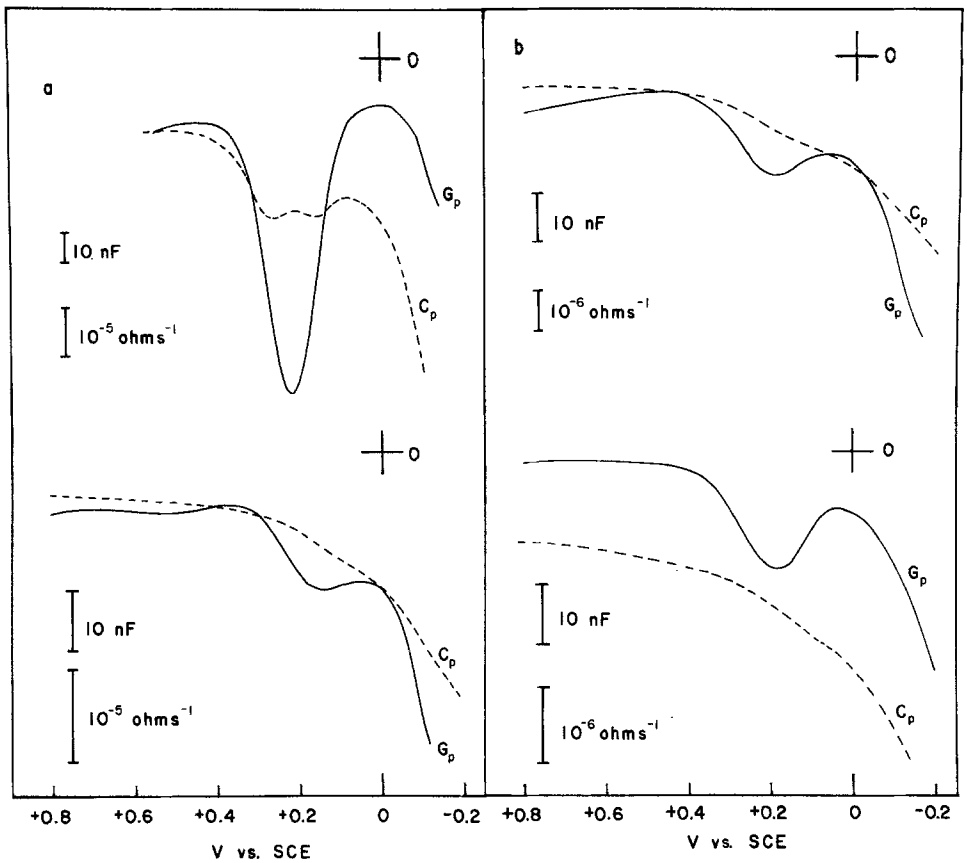

Fig. 2. AC impedance of n-$MoSe_2$ in 0.2M $K_4Fe(CN)_6$. (a) and (b) denote different electrodes. The upper plots are for 100 Hz, and the lower for 500 Hz. G_p, in-phase or equivalent parallel conductance, C_p; quadrature or equivalent parallel capacitance.

filtering. Since Δj is the differential photocurrent at any potential, information concerning inflections in the photocurrent attributable, for example, to surface recombination and surface states, are amplified in Δj. Even a very small dip or hump in j *vs.* V will be apparent in Δj *vs.* V plots. Recall that the in-phase component (Fig. 2) exhibits a peak in the same potential regime in which the j and Δj *vs.* V plots exhibit a hump. This observation suggests that the differential photocurrent technique can be used as a diagnostic tool to probe the electrode surface for surface states.

The ac impedance and current-voltage behavior of n-$MoSe_2$ after surface modification with RuO_x.—These techniques, in conjunction with the ac impedance and current-voltage measurements, have been extended to regimes where surface states can be passivated by a thin layer of RuO_x. The thermodynamic potential for RuO_x deposition from $Ru(\eta^6\text{-}C_6H_6)(OH_2)_3^{2+}$ complex is about +0.9V *vs.* SCE. The VB edge of n-$MoSe_2$ is located at

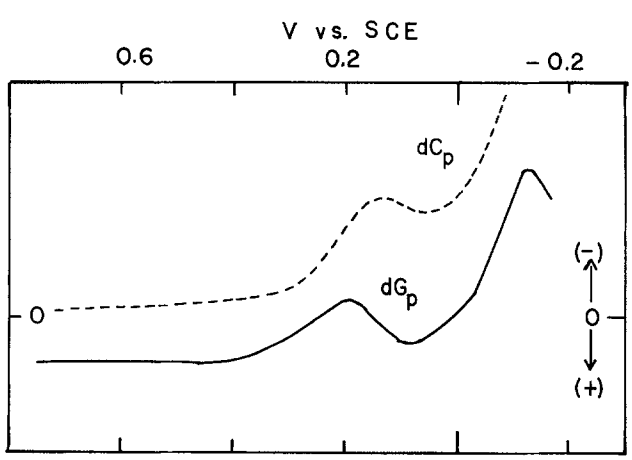

Fig. 3. Second harmonic ac impedance for n-$MoSe_2$ in aqueous 0.2M $K_4Fe(CN)_6$. Fundamental modulation frequency = 500 Hz. Sensitivity for dG_p (second harmonic of G_p) and dC_p (second harmonic of C_p) are 100x and 20x, respectively, G_p and C_p in Fig. 2b. Negative values are plotted upward.

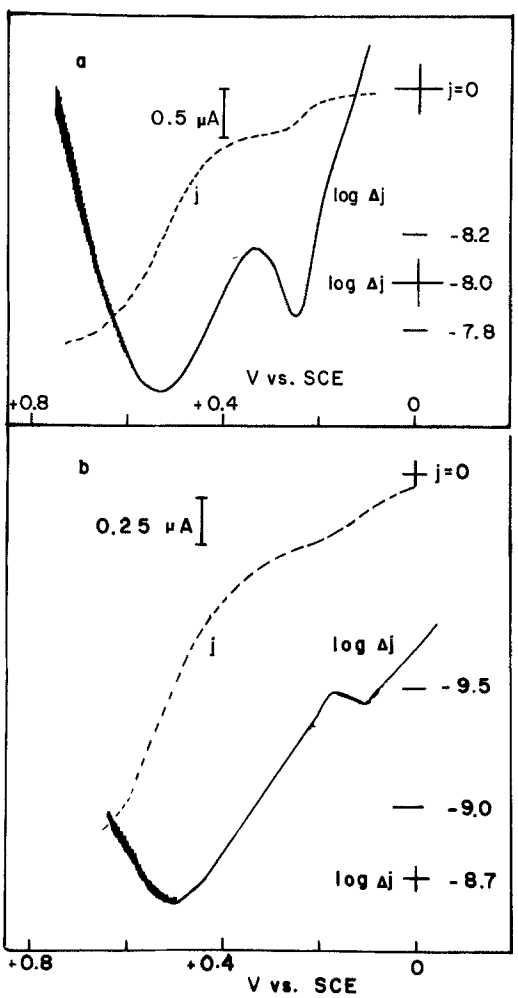

Fig. 4. Photocurrent (j) and log differential photocurrent (Δj) *vs.* potential for n-$MoSe_2$ in 0.2M $K_4Fe(CN)_6$. Monochromatic illumination at 500 nm, j obtained with light modulation at ~1.1 kHz, and Δj at the difference frequency (0.4 kHz) between the potential modulation (~1.5 kHz) and the light modulation. (a) and (b) denote different electrodes. The plots for (a) are for the electrode of Fig. 2a.

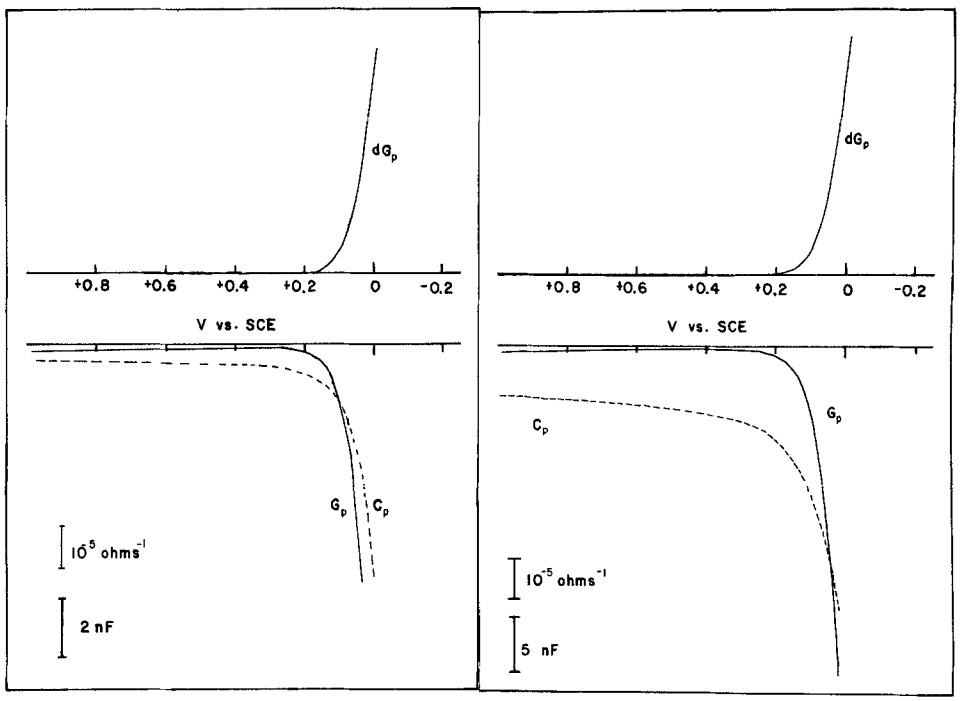

Fig. 5. AC impedance of n-$MoSe_2/RuO_x$ in 0.2M $K_4Fe(CN)_6$. G_p = equivalent parallel conductance, C_p = equivalent parallel capacitance, dG_p = second harmonic of G_p (sensitivity = 5 × G_p). Modulation frequency is 25 Hz (left) and 100 Hz (right). Negative values of dG_p are plotted upward.

1.16V *vs.* SCE. We have photoelectrochemically deposited a thin layer of RuO_x on the surface of the n-$MoSe_2$ electrode of Fig. 2a held at +0.5V under white light illumination from a 450W Xe lamp. The film appeared golden yellow, and the amount of charge passed was equal to 1.9 mC (~ 30 mC/cm²). In Fig. 5 are given plots of the impedance and the second harmonic ac impedance for two modulation frequencies in $K_4Fe(CN)_6$ solution. Both the ac impedance at the fundamental frequency and the more sensitive second harmonic exhibit smooth plots that are indicative of an improved surface. In Fig. 6 is shown the j and Δj *vs.* V for n-$MoSe_2$ after depositing RuO_x. Note the significant improvement in the shape of the current-voltage behavior. The photocurrent rises to saturation much more quickly than its counterpart in Fig. 4. This type of steep rise to saturation has been attributed to the absence of surface states and recombination effects (28, 29). At 0.3V, corresponding to the V_{redox} of $Fe(CN)_6^{4-/3-}$, the photocurrent (roughly corresponding to the short-circuit photocurrent in a two-electrode PEC cell configuration) of the RuO_x-modified electrode is approximately double that of the untreated electrode. Consider the behavior of the differential photocurrent. Δj decreases more sharply with V than its counterpart in Fig. 4. Further, the hump attributable to the presence of surface states is absent, suggesting the passivation of the surface states. The RuO_x films were found to be stable in the presence of all mineral acids, but could be dissolved by sulfochromic acid. Short treatments in this acid of bare n-$MoSe_2$ electrodes were found not to affect the ac impedance behavior. In Fig. 7 is given the plot of j and Δj *vs.* V after partially removing the RuO_x layer by briefly dipping the electrode in chromic acid. Compare Fig. 6 and 7. In both cases, the j *vs.* V behavior is the same. The lower photocurrent in Fig. 6 is probably due to larger attenuation of the impinging light intensity by a thicker RuO_x

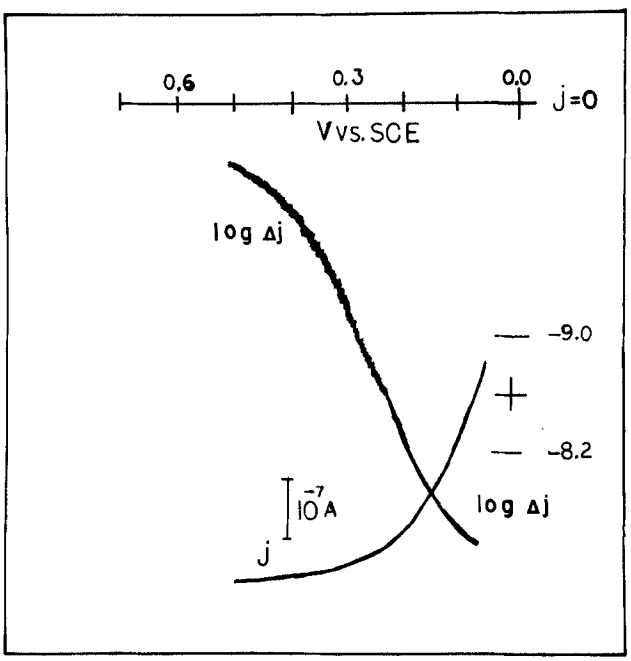

Fig. 6. Photocurrent (j) and log differential photocurrent (Δj) for n-$MoSe_2/RuO_x$ in 0.2M $K_4Fe(CN)_6$. Illumination and frequencies are as in Fig. 4.

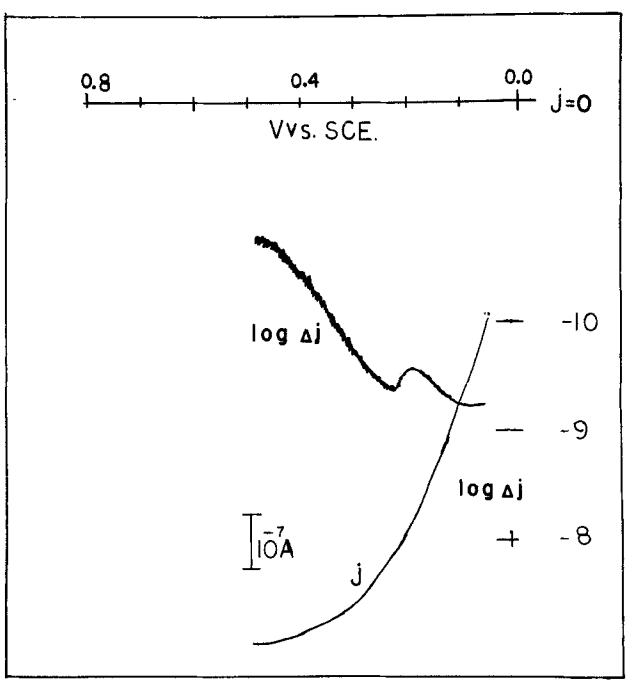

Fig. 7. Photocurrent (j) and log differential photocurrent (Δj) for n-$MoSe_2/RuO_x$ in 0.2M $K_4Fe(CN)_6$ after etching RuO_x coating in chromic acid for 5s. Monochromatic illumination and frequencies are as in Fig. 4.

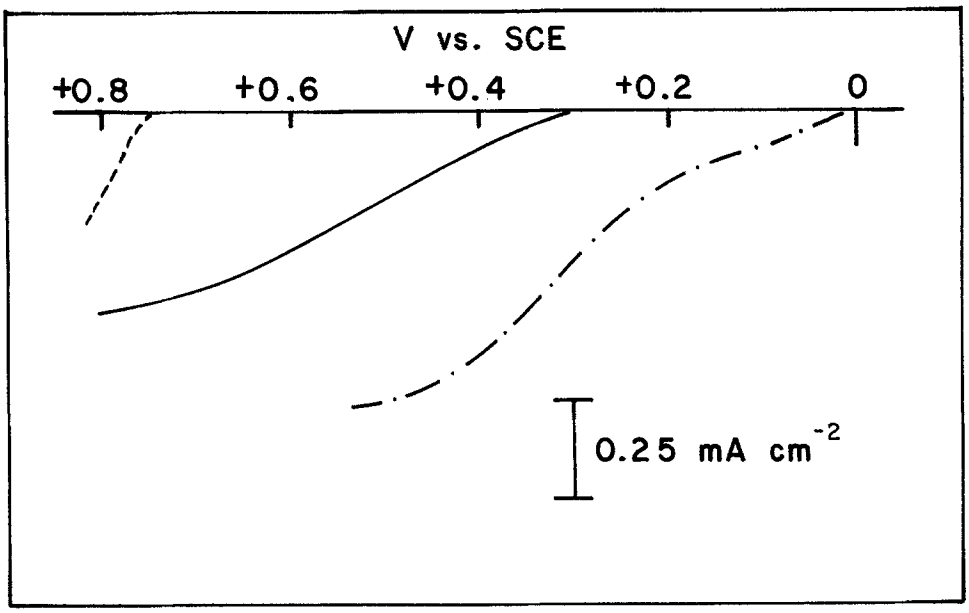

Fig. 8. Current-potential curves for smooth side of polycrystalline $MoSe_2$ in 1M KBr. Dark (---), illuminated with 450W Xe lamp (~100 mW/cm^2) (——), and after deposition of RuO_x under illumination (-·-).

film. However, the Δj *vs.* V behavior is not the same. This plot exhibits a hump in the same potential regime in which both the ac impedance and differential photocurrent (before RuO_x deposition) exhibit a hump. This observation indicates that the differential photocurrent method can be used to monitor the presence of surface states even at low levels, where the photocurrent behavior appears normal. In addition, even those states which cannot be charged in the dark but can be charged under illumination (30) are detectable by the differential photocurrent technique. In this respect it is even superior to the second harmonic impedance method for detecting surface states.

In a previous paper (14), we reported that the surface states existing on n-$MoSe_2$ were not present in sufficient density to cause pinning of the Fermi level in acetonitrile solutions. The possibility that a Schottky barrier exists between the n-$MoSe_2$ and the RuO_x is ruled out by the constant onset potential of photocurrent in solutions of iodide, bromide, and ferrocyanide. Formation of insulating layers such as oxides could cause the measured impedance to be no longer equivalent to the combination of space charge layer and surface states illustrated by Fig. A-1 of Ref. (14). The fact that RuO_x is a conducting layer, as well as the values of the capacitance away from the potential regime of the surface states before and after RuO_x deposition (compare Fig. 2a and Fig. 5), strongly suggests that the space charge layer capacitance is being measured. Additional support for this contention lies in the fact that even at frequencies as low as 100 Hz, the Mott-Schottky plots are linear; this would not be the case if the space charge capacitance were not approximately equivalent to the measured capacitance.

PEC behavior of polycrystalline n-$MoSe_2$.—Recent studies on polycrystalline films of p-WSe_2 (31) and n-WSe_2 (32) have been described. In the latter work, results of a modification procedure with silver and lanthanum ions were discussed. We report here work done on similar polycrystalline films of n-$MoSe_2$ and results of surface modification with photodeposited RuO_x films. In Fig. 8 is shown the j-V behavior for the smooth side of polycrystalline n-$MoSe_2$ in aqueous solution containing 1.0*M* KBr as the redox couple before and after depositing

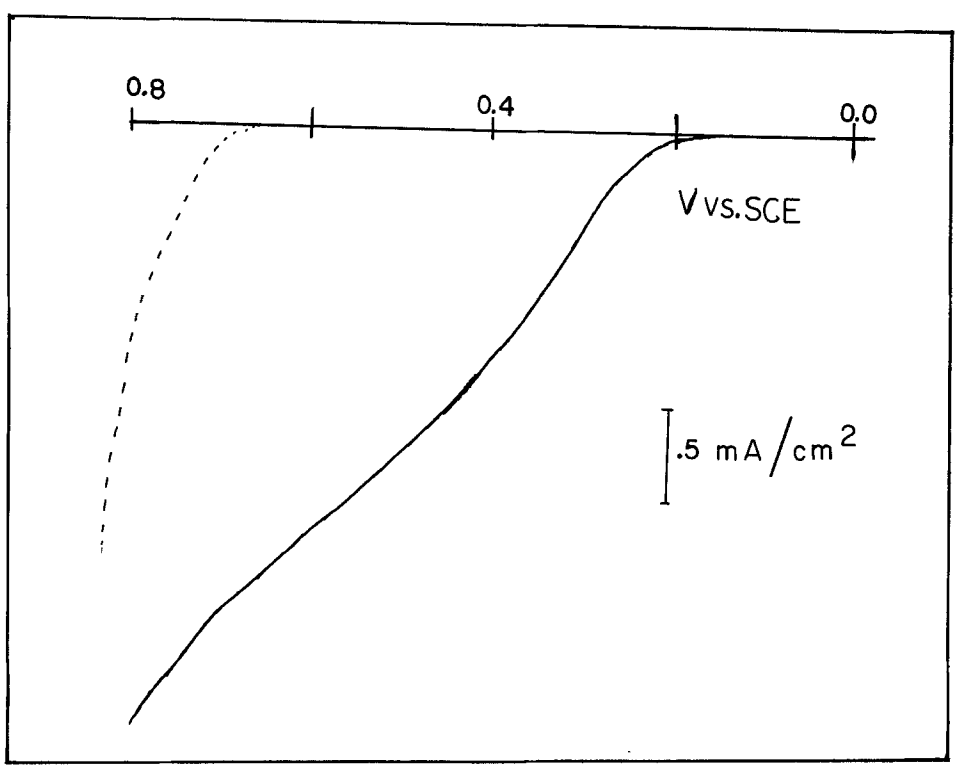

Fig. 9. Current-potential curves for rough surface of polycrystalline n-$MoSe_2$. Dark (---), illumination (——). Conditions are as in Fig. 8.

a thin layer of RuO_x. The conditions are the same as used for the single-crystal n-$MoSe_2$ except the number of coulombs passed in RuO_x deposition (~420 mC/cm² of projected surface area). (However, the actual surface area could be as much as an order of magnitude greater than the projected area.) The photoperformance is improved after RuO_x deposition; not only is the photocurrent increased, but the onset of photocurrent is located at least 0.3V more negative. Although the *j-V* performance appears to be improved after modifying the electrode surface with RuO_x, the photocurrent and efficiency of the polycrystalline material is still much smaller than that of treated single-crystal $MoSe_2$. Under similar conditions, the untreated rough side of the polycrystalline $MoSe_2$ gave better photocurrent than the RuO_x-coated smooth side (Fig. 9). However, deposition of the RuO_x on the rough side did not improve the behavior. Thus, the RuO_x treatment appears to help a poor surface more than a good one.

Conclusions

Both the second harmonic and the differential photocurrent methods can be used as diagnostic tools for monitoring the presence of surface states. Even under conditions where the presence of surface states cannot be detected by the photocurrent, the differential photocurrent can be used to detect them. Further, even those states which are not charged in the dark but can be charged under illumination can be detected by the differential photocurrent. In this respect, it is even superior to the second harmonic impedance method. The second harmonic is more sensitive than the ac impedance of the fundamental frequency.

Photoelectrodeposition of a thin film of RuO_x significantly improves both the potential for photocurrent onset as well as the short-circuit photocurrent for single-crystal n-$MoSe_2$ and the smooth side of polycrystalline $MoSe_2$. Attempts to study the behavior of similar n-$MoTe_2$ with RuO_x films were not successful. The $Ru(\eta^6\text{-}C_6H_6)(OH_2)_3^{2+}$ redox potential is more positive than the valence band-edge of this material (13) and, therefore, RuO_x films could not be formed by this method.

Acknowledgments

We are indebted to Dr. Barry Miller and Dr. Frank DiSalvo at AT&T Bell Laboratories for the gift of the sample of $MoSe_2$. The support of this research by the National Science Foundation (CHE8404666) and the Robert A. Welch Foundation is gratefully acknowledged. B. L. W. wishes to acknowledge the generous support of The Electrochemical Society, Inc., in the form of the Colin Garfield Fink Summer Fellowship.

Manuscript submitted Feb. 27, 1984; revised manuscript received May 14, 1984.

The University of Texas assisted in meeting the publication costs of this article.

REFERENCES

1. A. Heller and B. Miller, in "Interfacial Photoprocesses: Energy Conversion and Synthesis," M. S. Wrighton, Editor, p. 215, Advances in Chemistry Series 184, American Chemical Society, Washington, DC, (1980); M. S. Wrighton, in "Chemistry in Energy Production," symposium held December 10-12, 1980, New Orleans, LA, p. 25, Oak Ridge National Laboratory, Oak Ridge, TN (1982).
2. F.-R. F. Fan and A. J. Bard, *J. Am. Chem. Soc.*, **102,** 3677 (1980); A. J. Bard, F.-R. F. Fan, A. S. Gioda, G. Nagasubramanian, and H. S. White, *Disscus. Faraday Soc.*, **70,** 19 (1980).
3. S. N. Frank and A. J. Bard, *J. Am. Chem. Soc.*, **99,** 7427 (1975); P. Salvador and C. Gutierrez, *Chem. Phys. Lett.*, **86,** 131 (1982) and references therein; R. H. Wilson, *This Journal*, **127,** 228 (1980).
4. R. Haak and D. Tench, *ibid.*, **131,** 275 (1984).
5. R. N. Noufi, P. A. Kohl, S. N. Frank, and A. J. Bard, *ibid.*, **125,** 246 (1978).
6. H. Morisaki and K. Yazawa, *Appl. Phys. Lett.*, **33,** 1013 (1978).
7. Y. Nakato, A. Tsumura, and H. Tsubomura, *Chem. Phys. Lett.*, **85,** 387 (1982).
8. D. Laser and S. Gottesfeld, *This Journal*, **126,** 475 (1979).
9. H. Morisaki, M. Hariya, and K. Yazawa, *Appl. Phys. Lett.*, **30,** 7 (1977).
10. M. A. Butler and D. S. Ginley, *ibid.*, **42,** 582 (1983).
11. K. Kobayashi, Y. Aikawa, and M. Sukigara, *Chem. Lett.*, 679 (1981).
12. E. Kamieniecki, *J. Appl. Phys.*, **54,** 6481 (1983).
13. G. Nagasubramanian, B. L. Wheeler, G. A. Hope, and A. J. Bard, *This Journal*, **130,** 385 (1983).
14. G. Nagasubramanian, B. L. Wheeler, and A. J. Bard, *ibid.*, **130,** 1680 (1983).
15. D. P. Anderson and L. F. Warren, *ibid.*, **131,** 347 (1984).
16. R. A. Zelonka and M. C. Baird, *Can. J. Chem.*, **50,** 3063 (1972).
17. T. Sukegawa, T. Watanabe, T. Mizuki, and A. Tanaka, *IEEE Trans. Electron Devices*, **ed-27,** 1251 (1980).
18. B. L. Wheeler, G. Nagasubramanian, and A. J. Bard, *This Journal*, **131,** 1038 (1984).
19. H. Tributsch, H. Gerischer, C. Clemen, and E. Bucher, *Ber. Bunsenges. Phys. Chem.*, **83,** 655 (1979).
20. P. K. Vasudev, B. L. Mattes, E. Pietras, and R. H. Bube, *Solid State Electron.*, **19,** 557 (1976).
21. J. Bardeen, *Phys. Rev.*, **71,** 717 (1947).
22. A. J. Bard, A. B. Bocarsly, F.-R. F. Fan, E. G. Walton, and M. S. Wrighton, *J. Am. Chem. Soc.*, **102,** 3671 (1980).
23. E. H. Nicollian and A. Goetzberger, *Bell Syst. Tech. J.*, **46,** 1055 (1967).
24. M. Abe, H. Morisake, and K. Yazawa, *Jpn. J. Appl. Phys.*, **19,** 1421 (1980).
25. J. A. Copeland, *IEEE Trans. Electron Devices*, **ed-16,** 445 (1969).
26. C. L. Anderson, R. Baron, and C. R. Crowell, *Rev. Sci. Instrum.*, **47,** 1366 (1976).
27. K. H. Zaininger and F. P. Heiman, *Solid State Technol.*, **13,** 46 (1970).
28. M. P. Dare-Edwards and A. Hamnett, *J. Electroanal. Chem.*, **105,** 283 (1979).
29. J. Gobrecht and H. Gerischer, *Solar Energy Mater.*, **2,** 131 (1979); D. Laser and A. J. Bard, *This Journal*, **123,** 1828 (1976).
30. G. Cooper, J. A. Turner, B. A. Parkinson, and A. J. Nozik, *J. Appl. Phys.*, **54,** 6463 (1983).
31. H. D. Abruna and A. J. Bard, *This Journal*, **129,** 673 (1982).
32. D. S. Ginley, R. M. Biefield, B. A. Parkinson, and K. Keung-Kam, *ibid.*, **129,** 145 (1982).